Quantitative, super-resolution localization of small RNAs with sRNA-PAINT

Kun Huang [1,2], Feray Demirci [3], Mona Batish[4], Blake C. Meyers [5,6*], Jeffrey L. Caplan [1,2*]

[1] Department of Plant and Soil Sciences, University of Delaware, Newark, DE 19716, USA

[2] Bio-Imaging Center, Delaware Biotechnology Institute, University of Delaware, Newark, DE 19716, USA

[3] FiDoSoft Software Consulting, Redmond, WA, 98052, USA

[4] Department of Medical and Molecular Sciences, University of Delaware, Newark, DE 19716

[5] Donald Danforth Plant Science Center, 975 North Warson Road, St. Louis, Missouri 63132, USA

[6] University of Missouri – Columbia, Division of Plant Sciences, 52 Agriculture Lab, Columbia, MO 65211

* To whom correspondence should be addressed: Jeffrey L. Caplan; Tel: (302) 831-3403; Fax: (302) 831-4841; Email: jcaplan@udel.edu

Correspondence may also be addressed to: Blake C. Meyers; Tel: (314) 587-1422; Email: bmeyers@danforthcenter.org

Keywords

Small RNA, RNA detection, DNA-PAINT, *in situ* hybridization, super-resolution, single molecule, microscopy, maize anther, quantification

Abstract

Small RNAs are non-coding RNAs that play important roles in the lives of both animals and plants. They are 21- to 24-nt in length and around 10 nanometers (nm) in size. Their small size and high diversity have made it challenging to develop detection methods that have sufficient resolution and specificity to multiplex and quantify. We created a method, sRNA-PAINT, for the detection of small RNAs with 20 nm resolution by combining the super-resolution method, DNA-based points accumulation in nanoscale topography (DNA-PAINT), and the specificity of locked nucleic acid (LNA) probes for the *in situ* detection of multiple small RNAs. The method relies on designing probes to target small RNAs that combine DNA oligonucleotides (oligos) for PAINT with LNA-containing oligos for hybridization; therefore, we developed an online tool called "Vetting & Analysis of RNA for *in situ* Hybridization probes" (VARNISH) for probe design. Our method utilizes advances in DNA-PAINT methodologies, including qPAINT for quantification, and Exchange-PAINT for multiplexing. We demonstrated these capabilities of sRNA-PAINT by detecting and quantifying small RNAs in different cell layers of early developmental stage maize anthers that are important for male sexual reproduction.

Introduction

In plants, 21- to 24-nucleotide (nt), non-coding small RNAs (sRNAs) regulate many important biological processes (1). Plant and animal genomes encode various sRNAs that can be divided into two major categories: microRNAs (miRNAs) and small interfering RNAs (siRNAs) (2). miRNAs are derived from long, hairpin precursor RNAs processed by precise cleavage, yielding mature miRNAs which influence gene transcript levels and translation (3). Plant siRNAs, also derived from long precursors that are made double-stranded by RNA-dependent RNA polymerases (RDRPs), are processed into mature siRNAs, and regulate gene transcript levels through post-transcriptional silencing, and epigenetically via RNA-directed DNA methylation (RdDM) (4). Some plant miRNAs trigger phased, secondary siRNAs (phasiRNAs), which are either 21 or 24 nt in length (5-7). Anthers, the plant male reproductive organ, are a particularly rich source of miRNAs and phasiRNAs, well-described in grasses including maize (7); during the meiotic stage, anthers are composed of cell layers that include the epidermis, endothecium, middle, and tapetum, that all surround the pollen mother cells. In maize anthers, the abundance and distribution of miRNAs and phasiRNAs vary in different cell layers (7), and our interest in the spatial organization and concentration of these sRNAs, particularly at the subcellular level, provided us a strong motivation to develop new methods for fluorescent detection.

33 sRNAs are mobile, moving within and between organelles, from cell-to-cell, and long distances within an
34 organism or even across organismal boundaries in plant-pathogen interactions (8). For example, within a
35 cell, sRNAs move between the nucleus and cytoplasm, bind Argonaute (AGO) proteins, Dicing bodies (D-
36 bodies), Cajal bodies (CBs), and may be polysome-associated or found with organelles such as the
37 endoplasmic reticulum (9-12). Intercellular movement of sRNAs, presumably via plasmodesmata in
38 plants, regulates tissue and organ development by silencing and regulating developmentally important
39 genes (13). Systemic translocation of sRNAs has been demonstrated by epigenetic silencing across graft
40 junctions and sRNA profiling of vasculature (8,14). Remarkably, sRNAs also move between organisms at
41 host-pathogen interfaces (15). Pathogens, including parasitic plants, regulate host defense responses via
42 miRNAs and *trans*-species sRNAs, and vice versa (16). In animals, extracellular vesicles (EVs) transport
43 miRNAs from cell-to-cell and over long-distances (17). Plant EVs are populated with miRNAs as well as
44 with fragments as small as 10 to 17 nt, so-called tiny RNAs (2). All of these sRNAs vary in abundance
45 from low to extremely high, as measured by sequencing, which typically utilizes gram quantities of plant
46 tissue, a process that substantially limits spatial analyses. At the subcellular level, the localizations of
47 these RNAs are not well-characterized. Thus, future approaches to sRNA characterization will require
48 nanometer resolution, high specificity, and both multiplexing and quantitative capabilities.
49
50 For *in situ* hybridization of sRNAs, the use of locked nucleic acid (LNA) oligonucleotide probes has shown
51 specificity and high fidelity (18). However, colorimetric and even fluorescent localization of sRNAs using
52 LNA-based methods are able to resolve only cell-level localization patterns. Because of the limits of light
53 diffraction, light microscopy cannot resolve spots below ~200 nm in diameter and 400 to 700 nm in axial
54 length (19). New techniques have been developed to drive microscopic detection beyond the diffraction
55 limit, yielding so-called "super-resolution" microscopy, such as Photo-Activated Localization Microscopy
56 (PALM), Structured Illumination Microscopy (SIM), direct Stochastic Optical Reconstruction Microscopy
57 (dSTORM), and Points Accumulation for Imaging in Nanoscale Topography (PAINT) (19). We have
58 previously demonstrated an sRNA-FISH method combined with SIM and dSTORM (20). However,
59 dSTORM utilizes the blinking property of fluorescent dyes and relies on specific excitation and buffer
60 conditions to achieve proper imaging (21). Photoswitching of the dye molecule is hard to predict, which
61 made absolute quantification difficult usingthe dSTORM method. The number of dyes with the
62 appropriate photoswitching properties within the visible spectrum is also a limiting factor for
63 multiplexed detection (21). DNA-PAINT decouples the blinking events from dye photophysics, using the
64 binding and dwelling kinetics of a short dye-labeled oligonucleotide "imager strand" to localize target-

65 specific “docking strands” (22,23). The docking strand in DNA-PAINT is linked to an antibody for single-
66 molecule protein detection, with imager strands introduced by perfusion, one imager strand at a time,
67 each specific to a given docking strand and protein. After the image is acquired, the imager strand is
68 washed off and then the next imager strand is introduced (21). As a result, a single dye can be linked to
69 different imager strands and applied for detection of numerous protein targets via use of different
70 imager strand-docking strand combinations. This multiplexing technique, known as “Exchange-PAINT”
71 has been used for *in situ* imaging of protein targets, such as microtubules and mitochondria (23), and *in*
72 *vitro* profiling of miRNAs using barcoded synthetic DNA origami (24).
73
74 To achieve subcellular, nanometer resolution imaging for the localization and analysis of sRNAs, we
75 created a detection method called sRNA-PAINT. This method combines the high resolution and precise
76 quantification of DNA-PAINT with the efficiency and specificity of LNA-based *in situ* hybridization. We
77 created a probe design tool for our method and show that these sRNA-PAINT probes can used for robust
78 sRNA detection. And, we have demonstrated that it can be combined with qPAINT to localize and
79 quantify distinct sRNAs in fixed biological sample, and with Exchange-PAINT for multiplexed target
80 detection.
81
82 **Materials and Methods**
83 *Plant materials and oligonucleotides.*
84 Maize anthers from W23 were provided by the Walbot lab at Stanford University (Palo Alto, CA). Plants
85 were grown in Palo Alto, CA under greenhouse conditions. Anther dissection and measurements were
86 performed as previously described (25). LNA-modified oligonucleotide probes were designed using our
87 VARNISH software and synthesized by Exiqon (QIAGEN; Germantown, MD). Imager strands coupled with
88 Alexa Fluor 647 (AF647) were ordered from IDT (Coralville, Iowa).
89
90 *Sample preparation.*
91 Sample preparation for *in situ* hybridization was performed as previously described (20). Briefly, anthers
92 were dissected and fixed in a 50 ml tube using 4% paraformaldehyde in 1xPHEM buffer (5 mM HEPES, 60
93 mM PIPES, 10 mM EGTA, 2 mM $MgSO_4$ at pH 7). Samples were then processed in a vacuum chamber
94 (0.08 MPa) three times, 15 min each. After fixation, samples were embedded in paraffin at the
95 Histochemistry and Tissue Processing Core Lab at Nemours/Alfred I. duPont Hospital for Children
96 (Wilmington, DE). Paraffin samples were sectioned at 6 µm thickness using a paraffin microtome and

97 dried on a Wide Spectral Band 600+/- 100 nm Gold Fiducials coverglass (600-100AuF; Hestzig LLC,
98 Leesburg, VA) at 37 °C degree on a slider warmer.
99
100 *In situ hybridization.*
101 The *in situ* hybridization step was performed following our previously-published protocol (20). Briefly,
102 samples were de-paraffinized using Histo-Clear (item 50-899-90147; Fisher Scientific, Pittsburgh, PA) and
103 re-hydrated by going through an ethanol series of 95, 80, 70, 50, 30, 10% (vol/vol) and water (1 min) at
104 room temperature. Then samples were treated with protease (item P5147; Sigma-Aldrich, St. Louis, MO)
105 for 20 min at 37°C. Excess formaldehyde background was removed by treating samples with 0.2%
106 glycine (item G8898; Sigma-Aldrich) for 20 min. After two washes in 1xPBS buffer (phosphate-buffered
107 saline), samples were dehydrated by going through an ethanol series of 10, 30, 50, 70, 80, 95%, and
108 100% (vol/vol). Hybridization was done with 10 µM probe at 53.3°C in a hybridization oven. After
109 hybridization, samples were washed twice with 0.2x SSC buffer (saline-sodium citrate). To immobilize
110 the hybridized probes, samples were incubated for 10 minutes in freshly prepared EDC solution
111 containing 0.13 M 1-methylimidazole, 300 nM NaCl (pH 8.0). Then samples were incubated for 1 hour
112 and 15 minutes in 0.16 M N-(3-Dimethylaminopropyl)-N'-ethylcarbodiimide hydrochloride (EDC) (item
113 03450, Sigma-Aldrich, St. Louis, MO) solution. Slides then were washed twice in TBS solution, 10 min
114 each wash. Hybridized samples were kept in 1xTBS at 4°C until imaging. smFISH was carried out as
115 previously described (26). 35 probes were used to detect the *PHAS* precursor lncRNA, as shown in
116 Supplementary Table 2. Quantification of smFISH was processed using SpotCounter program in ImageJ.
117 Three different spots from each layer, were used for quantification, which were the exact same
118 locations used in qPAINT quantification for direct comparison.
119
120 *Super-resolution imaging and image reconstruction.*
121 Super-resolution imaging was carried out on an inverted Zeiss Elyra PS.1 super-resolution microscope
122 (Carl Zeiss, Lberkochen, Germany). TIRF illumination was done using a 100% 642 nm laser and α-Plan-
123 Apochromat 100x/1.46 oil objective. For each imager strand, as well as control imager strand, images
124 were taken with an exposure time of 100 ms, an EMCCD Gain 30, and 20,000 frames in total.
125
126 Each image was analyzed and rendered in Zen software (Carl Zeiss Inc., Thornwood, NY). The images
127 were processed using the following identical parameters: Ignore overlapping molecules; Peak Mask Size
128 (6); Peak Intensity to Noise (6.0); Fit model (x,y 2D Gauss Fit). Drift correction was done by using fiducial-

129 based algorithm. For image rendering, pixel resolution was set to 16 nm/pixel and 2 nm/pixel for
130 zoomed in images with 1x and 0.5x PSF (point spread function) expansion factor. The number of
131 photons was selected between 420 and 10000 to eliminate non-specific background.
132
133 *sRNA-PAINT.*
134 A DH40iL culture dish incubate system (model 640388; Warner Instruments LLC, Hamden, CT) and a
135 quick release magnetic chamber for 25 mm low profile, round coverslips (model 641943; Warner
136 Instruments LLC) were assembled and used as the perfusion chamber. A ValveLink8.2 Perfusion System
137 (AutoMate Scientific, Berkeley, CA) was used for perfusing buffer and imager strand solutions and
138 washing solution into the chamber. ValveLink 8.2 perfusion system is a gravity force-driven perfusion
139 system. We used a working height about 15 cm above the imaging chamber. All imager strands were
140 diluted to 0.5-2 nM in buffer C (1× PBS, 500 mM NaCl, pH 8). Images were taken with constant flow of
141 imager stand. A Masterflex C/L peristaltic pump (60 RPM, model 77120-62; Cole-Parmer Instrument
142 Company LLC, Vernon Hills, IL) was used to constantly collect the waste buffer flow at maximum speed.
143
144 *sRNA-Exchange-PAINT.*
145 For multiplexed detection, all the probes were designed with VARNISH tool by picking different docking
146 and imager strand combinations. Following the same *in situ* hybridization procedure as described
147 earlier, each probe was denatured in an individual tube. After chilling on ice, all the probes were mixed
148 together and hybridized to the tissue simultaneously overnight at 53.3°C in a hybridization oven. The
149 probes were washed off with 0.2x SSC buffer the next morning, and stored in 1x PBS buffer till imaging.
150 DAPI (4',6-diamidino-2-phenylindole) stained nuclei images were taken after Exchange-PAINT.
151 Alignment of channels were done using TrakEM2 package of ImageJ (27). Probes used for multiplexed
152 detection are listed in Supplementary Table 1.
153
154 *Quantification of sRNA-qPAINT with Picasso software.*
155 qPAINT data analysis was performed following the protocol by Schnitzbauer et al. (21) and using the
156 Picasso software package. In brief, 8000 frames of the raw movie file of PAINT data were processed with
157 "Picasso: Localize". We adjusted the threshold until only the PAINT spots were detected and selected
158 (13000 Min Net Gradient was chosen for this manuscript). After "Localize (Identify & Fit)", a .hdf5 file
159 was generated and this was used as the input for the next module. The .hdf5 file was opened in
160 "Picasso: Render", and marker-based drift correction or redundant cross-correlative drift correction was

161 performed. We picked a 3.18 µm (20 pixel) diameter circle in the cytoplasm of each anther cell layer
162 using "Tools: Pick" and then performed qPAINT analysis with Picasso. The copy number in these picked
163 regions of each cell in each layer was used to calculate the number of binding sites in 63.25 μm^2, which
164 is roughly the area of the cytoplasm of cells in our sections. The influx rate was calculated using the
165 formula, $\xi = k_{on} \times c$, in which k_{on} represented the association constant of the imager strand ($1.5 * 10^6$
166 $(Ms)^{-1}$), and c represented the concentration of the imager strand. The dark time under "View: Show
167 info" and the calculated influx rate were used to calculate binding sites. A total of 150 sample areas
168 across three biological replicates were used to determine the background binding number. We observed
169 5.12 background binding sites for scrambled control LNA probe. As a result, the 5.12 background binding
170 sites were subtracted from all other qPAINT quantifications. For each sample, 10 locations for each cell
171 layer were used to calculate the binding sites.
172
173 *Small RNA library and data handling*
174 The details of the library are as follows: it is a maize small RNA library with GEO accession number
175 GSM1262527 that includes 24,145,201 genome-matched reads between the sizes of 18 and 34 nt. After
176 removing adapters and low-quality reads, small RNA reads length between 18 and 34 nt were mapped
177 back to the reference genome of maize, version AGPv4 (28). Abundances of small RNAs were normalized
178 to "TP10M" (transcripts per 10 million) based on the total count of genome-matched reads in the
179 library.
180
181 *sRNA sequences.*
182 All small RNA probe sequences and imager strands used are listed in Supplementary Table 1.
183
184 **Results**
185 ***sRNA-PAINT probe design***
186 Most eukaryotic sRNA sequences are between 21 to 24 nt in length. To perform sRNA-PAINT, we
187 designed a probe that is composed of three sequences: the probe backbone sequence with LNA bases,
188 the DNA-PAINT docking strand sequence, and a linker sequence that connects those two (Figure 1). The
189 probe design is the most critical step of the sRNA-PAINT method; to facilitate this process, we created
190 an online tool called VARNISH (Vetting & Analysis of RNA for *in situ* Hybridization probes) for automated
191 design of sRNA-PAINT probes (https://wasabi.ddpsc.org/~apps/varnish/). The tool requires the input of
192 a target sRNA sequence and the hybridization parameters (defaults provided), including sodium (50

193 mM), magnesium (0 mM) and temperature (25°C). VARNISH first will reverse complement the sRNA
194 sequence and will then choose between 19 and 22 nt of the sequence such that the melting point
195 temperature (T_m) is lower than 60°C, with preference for lower T_m values for the longest sequence
196 length. The melting temperature is calculated by using the "Analyze" function from the IDT web
197 application program interface (API) (https://www.idtdna.com/AnalyzerService/AnalyzerService.asmx).
198 The final sequence is the probe backbone (Figure 1, cyan). Next, LNA bases and a linker sequence are
199 introduced to the selected probe backbone by VARNISH. The default linker sequence is "tattcgt", which
200 has no match to the sRNA sequences in miRBase, but which can be changed to any desired custom linker
201 sequence. VARNISH introduces between five and nine LNA bases (default is eight) and it avoids stretches
202 of more than four LNA bases and three or more Gs or Cs. The algorithm exhausts all the possible
203 combinations of the positions for LNA bases, and it calculates the approximate T_m using previously
204 estimated T_m values for different LNAs (29). Next, VARNISH takes the top 200 probe backbone
205 candidates with the highest T_m and calculates the exact T_m using the IDT web API. The last step is to add
206 the DNA-PAINT docking strand. In the VARNISH tool, the docking strand can be either chosen from a
207 drop down menu containing the 13 previously used docking strands (23) or the sequence can be entered
208 manually in the VARNISH tool. The software will conduct a homo-dimer and secondary structure analysis
209 from all, or a subset of, the 13 provided docking strands in combination with the linker and the top 200
210 probe backbone candidates. These two steps are performed by using the "SelfDimer" and
211 "UNAFoldRun" functions from the IDT web API. Finally, the algorithm will choose the top 10 candidates
212 for each docking stand with the highest T_m and lowest ΔG for homo-dimer and secondary structure
213 predictions. Once the computations are complete, VARNISH will send an email message containing a
214 weblink to an output page that lists the 10 top probe candidates and information on ordering both the
215 probes and their corresponding imager strands.
216
217 ***sRNA-PAINT detects and quantifies cellular sRNAs at single molecule resolution***
218 Figure 1B shows the general process for the sRNA-PAINT method. First, the samples are fixed,
219 embedded in paraffin, and sectioned. Then, thin sections were placed onto coverslips with gold fiducials
220 sealed with silicon dioxide (SiO_2). The gold fiducials were used as alignment landmarks for image
221 registration over time and after buffer exchanges. We highly recommend that no additional coatings
222 are added, such as poly-l-lysine, since they resulted in non-specific binding. Next, during the
223 hybridization process, probes are applied to fixed and sectioned samples (Figure 1B). Excess probes are
224 removed in the washing process. Afterward, imager strands are perfused in. When the un-annealed

225 imager strands flow within the buffer, the speed of the movement is too fast to be caught by the
226 microscope. However, when an imager strand finds its docking partner, and dwells on it, the short time
227 period before the imager strand dissociates from the docking creates a blinking event that can be
228 detected using a total internal reflection fluorescence microscope (TIRFM). As a result, when thousands
229 of these blink events are collected, detection of all the docking sites within the sample is eventually
230 completed, defining the locations of the sRNA targets.
231
232 For sRNA-PAINT probe labeling, we selected Alexa Fluor 647 dye (AF647). First, AF647 emits far-red
233 fluorescence that is distinct from tissue autofluorescence; second, its photophysical property made it a
234 dye suitable for generating quality super-resolution images (30). The sRNA probes designed by VARNISH
235 were hybridized and the coverslip was mounted in a perfusion chamber. The corresponding, 3'-dye-
236 labeled imager strands were continuously perfused and imaging was conducted using TIRFM. As a
237 demonstration, we performed sRNA-PAINT on an abundant 24-nt phasiRNA – a class of plant secondary
238 siRNAs abundant in the early developmental stages of maize anthers (7) (Figure 2); the 24-nt phasiRNAs
239 are triggered by an miRNA, miR2275, providing us with two different classes of small RNAs in one tissue.
240 Our sRNA-PAINT experiment (Figure 2A) was consistent with our previous findings that the 24-nt
241 phasiRNA was present in all of the anther cell layers, and most abundant in the tapetum layer and pollen
242 mother cells (7) ; however, our, sRNA-PAINT approach achieved a much higher resolution of below 10
243 nm (Figure 2B).
244
245 qPAINT can count molecules by analyzing the predictable and programmable binding kinetics of the
246 imager strand to the docking strand (22). This quantitative method is based solely on binding kinetics,
247 and therefore, individual molecules do not need to be resolved. The Picasso software is publicly
248 available and can perform this calculation for the binding sites within a selected region (21). We then
249 performed qPAINT analysis on 24-nt phasiRNA with Picasso. As shown in Figure 2C, we detected 71.51
250 copies of 24-nt phasiRNA per selected region per cell in epidermal cells, 89.62 copies in endothecium
251 cells, 131.92 copies in middle layer cells, 199.92 copies in pollen mother cells, and most abundant,
252 209.86 copies in tapetal cells. These copy number values are minus the background detected in the
253 scrambled LNA control probe that was calculated to be 5.12 binding sites using 150 regions of images
254 from three biological replicates (Supplementary Figure 1). The scrambled LNA probe used to estimate
255 the non-specific binding of LNA probes has no similarity with maize small RNAs. Pollen mother cells and
256 tapetum have a greater abundance of the 24-nt phasiRNA compared with the other cell layers. qPAINT,

257 in combination with sRNA-PAINT, enabled the detection of the copy number of sRNAs in cell sections
258 and the sRNA targets in the different cell layers.
259
260 Next, we tested the specificity of the VARNISH probes and the essentiality of LNA bases. First, we tested
261 the specificity of the probe backbone by mutating 2 nucleotides in the 24-nt phasiRNA probe backbone.
262 As shown in Figure 2 and quantified in Supplementary Figure 2, the probe with the 2-nt mutation
263 detected very low background signal compared with the original probe, resulting in an average of 95%
264 decrease of the detected spots. Second, we confirmed that LNA is essential for efficient detection of
265 small RNA targets (18). We found that without LNA, the signal intensity is much lower compared with
266 probes with LNA (Figure 2) and nearly a 92% reduction in binding sites quantified by qPAINT
267 (Supplementary Figure 2). The scrambled, control LNA probe detected very little background
268 fluorescence (Supplementary Figure 1).
269
270 After the first round of imaging, buffer was perfused into the imaging chamber, and the signal was
271 diminished rapidly within 1 min, suggesting that stripping off the imager strand is very efficient. Next,
272 sRNA-PAINT signal was re-achieved by re-applying the imager strands (Figure 3A). We used EDC (1-ethyl-
273 1-(3-dimethylaminopropyl) carbodiimide) prior to imaging in order to cross-link and immobilize the
274 probes to prevent probe stripping during wash steps (31). After EDC treatment, the signal intensity in
275 the re-imaged sample was comparable with the original image (Figure 3A) and there was no significant
276 difference in quantified the number of binding sites (Figure 3B). Without EDC, there was a decrease in
277 image intensity after washing, as shown in Figure 3A and quantified in Figure 3B. The number of
278 localization spots detected remain relatively stable during the imaging process of 20,000 frames for
279 samples with or without EDC treatment (Supplementary Figure 3). We also confirmed that a different
280 imager strand had no or very little non-specific binding (Figure 3A), which is similar to the original DNA-
281 PAINT method (23).
282
283 ***Sequential multiplexed imaging of phasiRNA biogenesis components using sRNA-Exchange-PAINT***
284 Sequential detection of sRNAs can be performed by multiplexed VARNISH probes with different docking
285 strand combinations. We name this technique sRNA-Exchange-PAINT, as a variation of the protein-
286 focused, multiplexed Exchange-PAINT method. For this analysis, we measured both miR2275 and the
287 most abundant 24-nt phasiRNA it triggers, in maize anthers. As shown in Supplementary Figure 4, the
288 imager strand used for miR2275 (P0*) and 24-nt phasiRNA (P1*) do not non-specifically bind to each

289 other's docking strand. Sections on coverglass were mounted into a perfusion chamber and were first
290 perfused with P0* imager strand. After the image of miR2275 was acquired, buffer wash was performed
291 to completely remove the P0* imager strand. Next, the imager strand P1* was applied, and generated
292 the image for the 24-nt phasiRNA. Using traditional *in situ* hybridization methods, miR2275 and 24-nt
293 phasiRNA were thought to co-localize in the tapetum layer and pollen mother cells (7). Using sRNA-
294 PAINT, which has a resolution down to 10 nm, we confirmed that they co-localize to the tapetum layer
295 and pollen mother cells within the anther tissue, but we were not able to detect significant co-
296 localization at the level of single molecule analysis (Supplementary Figure 4B, zoomed image).
297
298 Higher levels of multiplexing can be achieved by sequential detection of multiple small RNA targets. To
299 achieve this, different docking strands could be attached to different sRNA-PAINT probe backbones by
300 simply specifying the choice of docking strand in the VARNISH software. All the sRNA-PAINT probes are
301 then hybridized to the tissue together in one hybridization step; after stringent washes, each imager
302 strand is perfused in for sequential detection of each target. We tested this high-level multiplexing with
303 the phasiRNA biogenesis components in 1 mm premeiotic maize anthers (Figure 5A). We aimed for four
304 components of the phasiRNA biogenesis pathways that shared the same precursor: miR2275, the *PHAS*
305 lncRNA precursor, and two phasiRNAs (5 phase "cycles" apart, or 5 x 24 nt = 120 nt apart). We also
306 included a fifth candidate, miR166, which regulates flower development but does not belong to the 24-
307 nt phasiRNA biogenesis pathway (32). Each of the five sRNA-PAINT probes, used at the same
308 concentration, was hybridized simultaneously to a maize anther cross-section (Figure 5A). We observed
309 effective detection of the targets by exchanging imager strands (Figure 5B); DAPI was subsequently
310 imaged as a counterstain for nuclei. In comparison with sRNA-seq data of multiple pooled 1 mm
311 anthers, quantification of each sRNA-PAINT channel showed similar trends in sRNA abundances (Figure
312 5C). Single-molecule resolution was preserved with high-level multiplexing (Figure 5D zoom)
313 demonstrating that sRNA-Exchange-PAINT preserved the quantification capability of qPAINT.
314
315 **Discussion**
316 sRNA-PAINT provides a robust method that quantitatively detects small RNAs with single-molecule
317 resolution. It greatly improves the resolution and precision of sRNA localization compared to other FISH
318 methods, namely those that are limited by the diffraction limit of light. The small size of sRNAs are
319 generally only detected by one probe per sRNA, as a result, each probe plays an important role with
320 respect to quantification. Our online VARNISH tool assists with the critical probe design step to generate

321 LNA probes with docking strands. Quantification of binding sites then can be deduced from the known
322 binding kinetics of the imager strands to the docking strands with sRNA-PAINT (22). A clear benefit of
323 sRNA-PAINT is ability to multiplex detection beyond three sRNAs, a capability that was previously
324 reserved for longer RNAs.
325
326 To develop a quantitative, super-resolution method for sRNA, we chose to design a PAINT-based
327 method over a dSTORM-based method for several reasons. The predictable binding of imager strands to
328 docking strands with PAINT-based method is preferred over the stochastic blinking of dye molecules in
329 dSTORM (22). Furthermore, quantification with a dSTORM probe using a single fluorophore molecule
330 would be greatly hindered by photobleaching. Bleached dye molecules would result in an
331 underestimation of the number of sRNA targets (20,33). In contrast, qPAINT-based methods are mostly
332 unaffected by fluorophore photobleaching because fluorophore molecules are constantly being
333 replenished by the binding of new imager strands (23). Rather, the major pitfall related to
334 photobleaching is photodamage of the docking strands during qPAINT-based methods caused by the
335 generation of reactive oxygen species (34). After EDC treatment, the photobleaching effect was
336 negligible for the highly abundant 24-nt phasiRNA, since there was no significant difference in the
337 qPAINT quantification after washing and reimaging (Figure 3). EDC has previously been shown to be
338 effective in the stabilization of redox status in treated mammalian tissue (35,36). Nonetheless, it should
339 be considered for future applications of sRNA-PAINT and it may be beneficial to use a reactive oxygen
340 scavenger buffer during image acquisition (34). Another possibility would be to combine sRNA-PAINT
341 with localization-based fluorescence correlation spectroscopy (lbFCS), rather than qPAINT, for absolute
342 molecular counting of sRNA (37).
343
344 An unforeseen benefit of using sRNA-PAINT is that it takes less time than regular *in situ* hybridization
345 methods. sRNA-PAINT samples are directly imaged after hybridization and washing, bringing the sample
346 preparation time down from 4 days to overnight (20). The rapidity was achieved via bypassing the
347 antibody incubation and amplification steps that typify those methods, including our previously
348 reported sRNA-FISH method (20). In sRNA-PAINT, the signal amplification occurs at the same time as
349 image acquisition; although, the drawback is that image acquisition for sRNA-PAINT takes longer than
350 traditional sRNA-FISH methods due to the need to take thousands of images for one field of view for
351 detection. Another benefit of bypassing the antibody amplification steps of traditional *in situ*
352 techniques is that the primary and secondary antibodies add significant amounts of bulk, decreasing the

353 precision of localization by 24 to 30 nm (38). Similarly, the original DNA-PAINT method utilized docking
354 strands conjugated to antibodies for protein detection (22,23,39). Overall, the sRNA-PAINT method
355 requires fewer steps than most comparable approaches and is relatively simple. The primary limitation
356 to sRNA-PAINT is the cost of the LNA oligos, which makes it expensive for new probes, although this cost
357 is amortized if the probe is used for many samples, as a typical yield for a purchased LNA oligo is enough
358 for hundreds to thousands of sRNA-PAINT experiments.
359
360 Colocalization data from sRNA-PAINT should be evaluated in the context of spatial information at the
361 tissue, subcellular, and molecular levels. In the case of miR2275 and the 24-nt phasiRNA, sRNA-PAINT
362 confirmed *in situ* hybridization data that showed these two sRNAs co-localize at the tissue level in
363 tapetal layer and pollen mother cells, and, at the subcellular level, mainly in the cytoplasm (7,20) .
364 However, at the molecular level, we observed minimal colocalization – evident because sRNA-PAINT has
365 single molecule resolution. The size of a small RNA is about 10 nm (40) and the imaging resolution of our
366 sRNA-PAINT is sub-20 nm. Co-localization of miR2275 and phasiRNA it triggered at the molecular level
367 would suggest that they physically interact with each other or that their density is too high for the
368 method to resolve individual target sRNA molecules; neither of which is apparently the case. In general,
369 colocalization at the single molecule level is plagued by potential imaging artifacts, such as sample drift
370 and sample distortion of deparaffinized sections during repetitive wash and imaging steps. We used the
371 gold fiducials immobilized on coverglasses for lateral image registration and autofocus to correct axial
372 drift; however, these approaches will not solve issues caused by sample damage and distortion over
373 time. Our plans include overcoming these limitations, mainly by mitigating sample distortion, so that
374 colocalization analysis of sRNA-PAINT can be used for sRNA-mRNA (messenger RNA) and sRNA-protein
375 interactions to examine outstanding questions in sRNA biogenesis and processing.
376
377 sRNA-PAINT was specifically developed for sRNA, which are too small to apply methods like smFISH that
378 are widely applied for longer mRNAs or lncRNAs. However, here we show that sRNA-PAINT can be used
379 for longer RNAs, but with some caveats. Compared to smFISH, the sRNA-PAINT method detected twice
380 as many copies of *PHAS* lncRNA. Qualitatively, sRNA-PAINT detected binding sites in areas that
381 appeared as diffuse fluorescence by smFISH. We hypothesize that sRNA-PAINT detected both the full
382 length *PHAS* lncRNA and the 5'cleaved products (Figure 4A). These degradation products will have fewer
383 binding sites for smFISH probes and may not result in discrete, bright spots. Therefore, we concede that
384 smFISH is a superior method for quantifying full-length, longer RNAs and should be used for that

385 application. sRNA-PAINT is best suited for multiplexing the detection of longer RNAs with sRNAs or to
386 study the processing of longer RNAs. Improvements in colocalization described above, combined with
387 multiplexing, may lead to powerful advancements in the sRNA-PAINT approach to study sRNA
388 biogenesis from longer precursors. Indeed, the limited number of experiments conducted to develop
389 sRNA-PAINT has led to new hypotheses. For example, we detected a higher number of binding sites for
390 *PHAS* lncRNA than its derivative 24 nt phasiRNA 2. One possibility is the probes detecting mature
391 phasiRNA-2 failed to detect the *PHAS* lncRNA precursor, as that region of the precursor may be
392 predominantly present as dsRNA. As suggested above, another possibility is that the cleaved 5' portion
393 of the *PHAS* precursor accumulates in the cells after AGO1-directed cleavage (Figure 4).
394
395 A distinct advantage of sRNA-PAINT is that it is compatible with Exchange-PAINT, for multiplexing using
396 multiple docking strands that are linked to the same fluorophore (23). Our previously described sRNA-
397 FISH method (20) is limited to only two to three targets, mainly due to the limited choices of antibodies
398 and fluorophores. Achieving the theoretical level of multiplexing for protein detection is mostly limited
399 by the number of primary and secondary antibodies. Our antibody-free method for sRNAs potentially
400 can achieve the theoretical level of multiplexing by designing hundreds of sRNA-PAINT VARNISH probes
401 to query numerous targets in the same sample. The current barriers of reaching the full potential of
402 sRNA-PAINT are the cost of LNA probes and the imaging time. These barriers may soon be removed as
403 the cost of LNA probes has been decreasing and new methods for increasing the speed of PAINT-based
404 methods have been developed (39,41). However, sRNA-PAINT, as currently conceived, will not reach the
405 same level of other highly multiplexed barcoding methods for mRNAs, such as MERFISH and seqFISH+.
406 MERFISH enabled multiplexed detection of 100 to 1000 RNA species in a single cell using a combination
407 of encoding probes and readout probes (42). The seqFISH+ method was able to detect 10,000
408 transcripts with high accuracy (43). Our main limitation is the small size of sRNAs. They are simply too
409 small to barcode with non-LNA probes. LNA probes are required for sRNA-PAINT (Figure 2), and high-
410 level multiplexing may be hindered by their cost and the required higher hybridization (55 °C) and
411 stripping (90 °C) temperatures compared to DNA probes. One intriguing avenue to increase multiplexing
412 is to barcode the docking strands. Agasti et al. (44) tested the orthogonality of 52 docking sequences
413 and concluded that those docking sequences could be used as DNA-barcoded labeling probes for PAINT.
414 We anticipate that many advances in our sRNA-PAINT method will be driven by clever, new ways to
415 improve all PAINT-based methods by other research groups.
416

417 Finally, our sRNA-PAINT method provides an alternative to conventional sRNA-FISH, as it is capable of
418 higher resolution, quantification, and multiplexing. All FISH-based methods are dependent on the actual
419 hybridization efficiency of the probes prior to imaging. sRNA-PAINT method still retains the pros and
420 cons of any LNA-based in situ method and that PAINT technology quantification is restricted to the
421 number of binding sites (hybridized probes). The development of LNA technology increased the
422 specificity and efficiency of sRNA-FISH methods making the development of sRNA-PAINT possible.
423 Future improvements in probes, such as the use of next-gen bridged nucleic acids (BNAs) (45) may
424 provide more efficient and specific labeling of target sRNAs that will benefit all FISH-based RNA
425 detection methods, including sRNA-PAINT. A drawback of the sRNA-PAINT method is that it can only be
426 applied to fixed tissues or cells. Live-cell imaging, especially aptamer-based sensor imaging for small
427 RNAs, was made possible by fluorescent RNA aptamers such as Spinach and Mango (46-48); however,
428 these methods have low sensitivity and resolution. Creating a live-cell sRNA-PAINT approach with single
429 molecule sensitivity would shed light on the dynamics and ever-changing contents of cellular RNAs.
430

431 **Acknowledgements**

432 This project was supported by the US NSF Plant Genome Research Program, awards 1649424, 1611853
433 and 1754097. We thank members of the Meyers and Caplan labs for help and support. We thank
434 Virginia Walbot (Stanford University) and members of her lab for supplying maize materials and for
435 useful discussions on another small RNAs. We thank Prof. Dr. Ralf Jungmann for his support in DNA-
436 PAINT, qPAINT and analysis with Picasso. Microscopy equipment was acquired with a shared
437 instrumentation grant (S10 OD016361) and access was supported by the NIH-NIGMS (P20 GM103446),
438 the NSF (IIA-1301765) and the State of Delaware.

439 **References**

440 1. Lewsey, M.G., Hardcastle, T.J., Melnyk, C.W., Molnar, A., Valli, A., Urich, M.A., Nery, J.R.,
441 Baulcombe, D.C. and Ecker, J.R. (2016) Mobile small RNAs regulate genome-wide DNA
442 methylation. *Proc Natl Acad Sci U S A*, **113**, E801-810.
443 2. Baldrich, P., Rutter, B.D., Karimi, H.Z., Podicheti, R., Meyers, B.C. and Innes, R.W. (2019) Plant
444 Extracellular Vesicles Contain Diverse Small RNA Species and Are Enriched in 10-to 17-
445 Nucleotide "Tiny" RNAs. *Plant Cell*, **31**, 315-324.
446 3. Wight, C., Ross, D.A. and Weinberger, D.R. (2018) Small RNAs May Answer Big Questions in
447 Mental Illness. *Biological Psychiatry*, **83**, E1-E3.
448 4. Borges, F. and Martienssen, R.A. (2015) The expanding world of small RNAs in plants. *Nature*
449 *Reviews Molecular Cell Biology*, **16**, 727-741.
450 5. Fei, Q., Xia, R. and Meyers, B.C. (2013) Phased, secondary, small interfering RNAs in
451 posttranscriptional regulatory networks. *Plant Cell*, **25**, 2400-2415.
452 6. Xia, R., Chen, C.J., Pokhrel, S., Ma, W.Q., Huang, K., Patel, P., Wang, F.X., Xu, J., Liu, Z.C., Li, J.G. *et*
453 *al.* (2019) 24-nt reproductive phasiRNAs are broadly present in angiosperms. *Nature*
454 *Communications*, **10**, 1-8.
455 7. Zhai, J.X., Zhang, H., Arikit, S., Huang, K., Nan, G.L., Walbot, V. and Meyers, B.C. (2015)
456 Spatiotemporally dynamic, cell-type-dependent premeiotic and meiotic phasiRNAs in maize
457 anthers. *P Natl Acad Sci USA*, **112**, 3146-3151.
458 8. Chitwood, D.H. and Timmermans, M.C.P. (2010) Small RNAs are on the move. *Nature*, **467**, 415-
459 419.
460 9. Fang, Y.D. and Spector, D.L. (2007) Identification of nuclear dicing bodies containing proteins for
461 microRNA biogenesis in living Arabidopsis plants. *Current Biology*, **17**, 818-823.
462 10. Li, C.F., Pontes, O., El-Shami, M., Henderson, I.R., Bernatavichute, Y.V., Chan, S.W.L., Lagrange,
463 T., Pikaard, C.S. and Jacobsen, S.E. (2006) An ARGONAUTE4-containing nuclear processing center
464 colocalized with Cajal bodies in Arabidopsis thaliana. *Cell*, **126**, 93-106.
465 11. Li, S.B., Le, B., Ma, X., Li, S.F., You, C.J., Yu, Y., Zhang, B.L., Liu, L., Gao, L., Shi, T. *et al.* (2016)
466 Biogenesis of phased siRNAs on membrane-bound polysomes in Arabidopsis. *Elife*, **5**, 1-24.
467 12. Song, L., Han, M.H., Lesicka, J. and Fedoroff, N. (2007) Arabidopsis primary microRNA processing
468 proteins HYL1 and DCL1 define a nuclear body distinct from the Cajal body. *P Natl Acad Sci USA*,
469 **104**, 5437-5442.
470 13. Dunoyer, P., Melnyk, C., Molnar, A. and Slotkin, R.K. (2013) Plant Mobile Small RNAs. *Cold Spring*
471 *Harbor Perspectives in Biology*, **5**, 1-3.
472 14. Yoo, B.C., Kragler, F., Varkonyi-Gasic, E., Haywood, V., Archer-Evans, S., Lee, Y.M., Lough, T.J. and
473 Lucas, W.J. (2004) A systemic small RNA signaling system in plants. *Plant Cell*, **16**, 1979-2000.
474 15. Johnson, N.R. and Axtell, M.J. (2019) Small RNA warfare: exploring origins and function of trans-
475 species microRNAs from the parasitic plant Cuscuta. *Curr Opin Plant Biol*, **50**, 76-81.
476 16. Cai, Q., Qiao, L.L., Wang, M., He, B.Y., Lin, F.M., Palmquist, J., Huang, S.N.D. and Jin, H.L. (2018)
477 Plants send small RNAs in extracellular vesicles to fungal pathogen to silence virulence genes.
478 *Science*, **360**, 1126-1129.
479 17. Liu, T., Zhang, Q., Zhang, J.K., Li, C., Miao, Y.R., Lei, Q., Li, Q.B. and Guo, A.Y. (2019) EVmiRNA: a
480 database of miRNA profiling in extracellular vesicles. *Nucleic acids research*, **47**, D89-D93.
481 18. Javelle, M. and Timmermans, M.C.P. (2012) In situ localization of small RNAs in plants by using
482 LNA probes. *Nature Protocols*, **7**, 533-541.
483 19. Hell, S.W. (2009) Microscopy and its focal switch. *Nat Methods*, **6**, 24-32.
484 20. Huang, K., Baldrich, P., Meyers, B.C. and Caplan, J.L. (2019) sRNA-FISH: versatile fluorescent in
485 situ detection of small RNAs in plants. *Plant Journal*, **98**, 359-369.

486 21. Schnitzbauer, J., Strauss, M.T., Schlichthaerle, T., Schueder, F. and Jungmann, R. (2017) Super-
487 resolution microscopy with DNA-PAINT. *Nature Protocols*, **12**, 1198-1228.
488 22. Jungmann, R., Avendano, M.S., Dai, M.J., Woehrstein, J.B., Agasti, S.S., Feiger, Z., Rodal, A. and
489 Yin, P. (2016) Quantitative super-resolution imaging with qPAINT. *Nat Methods*, **13**, 1198-1228.
490 23. Jungmann, R., Avendano, M.S., Woehrstein, J.B., Dai, M.J., Shih, W.M. and Yin, P. (2014)
491 Multiplexed 3D cellular super-resolution imaging with DNA-PAINT and Exchange-PAINT. *Nat*
492 *Methods*, **11**, 313-318.
493 24. Xu, W.D., Yin, P. and Dai, M.J. (2018) Super-resolution Geometric Barcoding for Multiplexed
494 miRNA Profiling. *Angewandte Chemie-International Edition*, **57**, 14075-14079.
495 25. Kelliher, T. and Walbot, V. (2011) Emergence and patterning of the five cell types of the Zea
496 mays anther locule. *Developmental biology*, **350**, 32-49.
497 26. Batish, M., Raj, A. and Tyagi, S. (2011) Single molecule imaging of RNA in situ. *Methods in*
498 *molecular biology*, **714**, 3-13.
499 27. Cardona, A., Saalfeld, S., Schindelin, J., Arganda-Carreras, I., Preibisch, S., Longair, M., Tomancak,
500 P., Hartenstein, V. and Douglas, R.J. (2012) TrakEM2 Software for Neural Circuit Reconstruction.
501 *Plos One*, **7**, 1-8.
502 28. Portwood, J.L., 2nd, Woodhouse, M.R., Cannon, E.K., Gardiner, J.M., Harper, L.C., Schaeffer,
503 M.L., Walsh, J.R., Sen, T.Z., Cho, K.T., Schott, D.A. *et al.* (2019) MaizeGDB 2018: the maize multi-
504 genome genetics and genomics database. *Nucleic acids research*, **47**, D1146-D1154.
505 29. McTigue, P.M., Peterson, R.J. and Kahn, J.D. (2004) Sequence-dependent thermodynamic
506 parameters; for locked nucleic acid (LNA)-DNA duplex formation. *Biochemistry*, **43**, 5388-5405.
507 30. Dempsey, G.T., Vaughan, J.C., Chen, K.H., Bates, M. and Zhuang, X.W. (2011) Evaluation of
508 fluorophores for optimal performance in localization-based super-resolution imaging. *Nat*
509 *Methods*, **8**, 1027-1036.
510 31. Pena, J.T.G., Sohn-Lee, C., Rouhanifard, S.H., Ludwig, J., Hafner, M., Mihailovic, A., Lim, C.,
511 Holoch, D., Berninger, P., Zavolan, M. *et al.* (2009) miRNA in situ hybridization in formaldehyde
512 and EDC-fixed tissues. *Nat Methods*, **6**, 139-141.
513 32. Sun, W., Chen, D., Xue, Y., Zhai, L., Zhang, D., Cao, Z., Liu, L., Cheng, C., Zhang, Y. and Zhang, Z.
514 (2019) Genome-wide identification of AGO18b-bound miRNAs and phasiRNAs in maize by cRIP-
515 seq. *BMC genomics*, **20**, 656-667.
516 33. Sehayek, S., Gidi, Y., Glembockyte, V., Brandao, H.B., Francois, P., Cosa, G. and Wiseman, P.W.
517 (2019) A High-Throughput Image Correlation Method for Rapid Analysis of Fluorophore
518 Photoblinking and Photobleaching Rates. *Acs Nano*, **13**, 11955-11966.
519 34. Blumhardt, P., Stein, J., Mucksch, J., Stehr, F., Bauer, J., Jungmann, R. and Schwille, P. (2018)
520 Photo-Induced Depletion of Binding Sites in DNA-PAINT Microscopy. *Molecules*, **23**.
521 35. Tamura, M., Tamura, T., Burnham, D.N., Uhlinger, D.J. and Lambeth, J.D. (1989) Stabilization of
522 the superoxide-generating respiratory burst oxidase of human neutrophil plasma membrane by
523 crosslinking with 1-ethyl-3-(3-dimethylaminopropyl) carbodiimide. *Archives of biochemistry and*
524 *biophysics*, **275**, 23-32.
525 36. Tamura, M., Takeshita, M., Curnutte, J.T., Uhlinger, D.J. and Lambeth, J.D. (1992) Stabilization of
526 human neutrophil NADPH oxidase activated in a cell-free system by cytosolic proteins and by 1-
527 ethyl-3-(3-dimethylaminopropyl) carbodiimide. *The Journal of biological chemistry*, **267**, 7529-
528 7538.
529 37. Stein, J., Stehr, F., Schueler, P., Blumhardt, P., Schueder, F., Mucksch, J., Jungmann, R. and
530 Schwille, P. (2019) Toward Absolute Molecular Numbers in DNA-PAINT. *Nano letters*, **19**, 8182-
531 8190.

532 38. Pleiner, T., Bates, M., Trakhanov, S., Lee, C.T., Schliep, J.E., Chug, H., Bohning, M., Stark, H.,
533 Urlaub, H. and Gorlich, D. (2015) Nanobodies: site-specific labeling for super-resolution imaging,
534 rapid epitope-mapping and native protein complex isolation. *Elife*, **4**, 1-21.
535 39. Schueder, F., Stein, J., Stehr, F., Auer, A., Sperl, B., Strauss, M.T., Schwille, P. and Jungmann, R.
536 (2019) An order of magnitude faster DNA-PAINT imaging by optimized sequence design and
537 buffer conditions. *Nat Methods*, **16**, 1101-1104.
538 40. Yoffe, A.M., Prinsen, P., Gopal, A., Knobler, C.M., Gelbart, W.M. and Ben-Shaul, A. (2008)
539 Predicting the sizes of large RNA molecules. *P Natl Acad Sci USA*, **105**, 16153-16158.
540 41. Filius, M., Cui, T.J., Ananth, A.N., Docter, M.W., Hegge, J.W., van der Oost, J. and Joo, C. (2020)
541 High-Speed Super-Resolution Imaging Using Protein-Assisted DNA-PAINT. *Nano letters*, **20**,
542 2264-2270.
543 42. Chen, K.H., Boettiger, A.N., Moffitt, J.R., Wang, S. and Zhuang, X. (2015) Spatially resolved, highly
544 multiplexed RNA profiling in single cells. *Science*, **348**, 1-14.
545 43. Eng, C.L., Lawson, M., Zhu, Q., Dries, R., Koulena, N., Takei, Y., Yun, J., Cronin, C., Karp, C., Yuan,
546 G.C. *et al.* (2019) Transcriptome-scale super-resolved imaging in tissues by RNA seqFISH. *Nature*,
547 **568**, 235-239.
548 44. Agasti, S.S., Wang, Y., Schueder, F., Sukumar, A., Jungmann, R. and Yin, P. (2017) DNA-barcoded
549 labeling probes for highly multiplexed Exchange-PAINT imaging. *Chemical science*, **8**, 3080-3091.
550 45. Soler-Bistue, A., Zorreguieta, A. and Tolmasky, M.E. (2019) Bridged Nucleic Acids Reloaded.
551 *Molecules*, **24**, 1-17.
552 46. Autour, A., Jeng, S.C.Y., Cawte, A.D., Abdolahzadeh, A., Galli, A., Panchapakesan, S.S.S., Rueda,
553 D., Ryckelynck, M. and Unrau, P.J. (2018) Fluorogenic RNA Mango aptamers for imaging small
554 non-coding RNAs in mammalian cells. *Nature Communications*, **9**, 1-12.
555 47. Huang, K., Doyle, F., Wurz, Z.E., Tenenbaum, S.A., Hammond, R.K., Caplan, J.L. and Meyers, B.C.
556 (2017) FASTmiR: an RNA-based sensor for in vitro quantification and live-cell localization of small
557 RNAs. *Nucleic acids research*, **45**, 1-13.
558 48. Paige, J.S., Wu, K.Y. and Jaffrey, S.R. (2011) RNA Mimics of Green Fluorescent Protein. *Science*,
559 **333**, 642-646.
560
561

562 **Figure Legends**

563 *Figure 1. Illustration of sRNA-PAINT probe design and workflow.*

564 (**A**) Illustration of a VARNISH probe design. A VARNISH probe is comprised of three parts: a probe
565 backbone (cyan) that is complementary to the target sRNA (orange), a docking strand (green) and a
566 linker sequence (dark blue) connecting them. The imager strand is conjugated to the fluorophore, and it
567 will find its corresponding docking strand during the imaging process. (**B**) A workflow for sRNA-PAINT.
568 Samples were fixed and embedded, and a thin section is placed on the coverglass. During the
569 hybridization process, the VARNISH probes will bind to sRNAs in the sample and locked with EDC. During
570 the imaging step, imager strands are added to the probe-hybridized sample on the coverglass.

571

572 *Figure 2. sRNA-PAINT detects 24 nt-phasiRNA specifically in an early-stage maize anther.*

573 (**A**) Detection of a 24-nt phasiRNA in a cross-section of maize anther. The VARNISH probe and modified
574 probes with either 2-nt mutations or the LNAs were applied to samples. 24-nt phasiRNA probes showed
575 signal while the mutation probe and no-LNA probe detected little to no signal. Scale bar = 10 µm in all
576 images. A red-to-white lookup table was used to display low-to-high intensity values. Arrows indicate 2
577 out of ~66 fiducials used in experiments. (**B**) Zoomed images of boxes 1 and 2 in panel A. There are more
578 24-nt phasiRNA localization events in the pollen mother cells (box 1) compared to the epidermal layer
579 (box 2). Expanded boxed areas (white) show representative areas at higher magnification, with centroid
580 positions shown in blue crosses. (**C**) qPAINT analysis of 24-nt phasiRNA in different anther cell layers.
581 Cartoon diagram representing each cell layer of a cross section of a maize anther lobe: epidermis
582 (yellow), endothecium (green), middle layer (red), tapetum (blue), and pollen mother cells (purple).
583 Numbers shows the binding events for each cell in all cytoplasmic areas of different cell layers. 10
584 different locations in each specified cell layer of three biological replicates were taken for statistical
585 analysis (n=150). Error bar indicates standard error for each sample.

586

587 *Figure 3. Comparison of sRNA-PAINT imaging and re-imaging with and without EDC treatment.*

588 (**A**) sRNA-PAINT imaging signal can be re-detected to a similar level when treated with EDC. Without EDC
589 treatment, re-imaged samples have lower fluorescence signal. A non-specific imager strand (last
590 column) was used as a control. Scale bar = 10 µm in all images. We used the same anther section used in
591 Figure 2. Arrows indicate 2 of the of ~66 fiducials used in experiments. (**B**) qPAINT analysis of image in
592 panel A. Numbers shows the binding events for each cell in different cell layers. 10 different locations in
593 each specified cell layer were taken for statistical analysis. Error bars indicate standard error for each

594 sample. Letters indicate significant differences using Tukey's test (P < 0.05, n=50). No significant
595 difference was observed in each cell layer during imaging and re-imaging in EDC treated samples.
596
597 *Figure 4. Application of sRNA-PAINT for detecting lncRNA transcript.*
598 (**A**) biogenesis pathway of phasiRNA in maize. AGO1-miR2275 cleaved *PHAS* lncRNA is produced into
599 long dsRNA via RDR6-SGS3. DCL5 cleaves target sites into 24-mers (phasiRNAs). Our sRNA-PAINT
600 suggests that AGO1-miR2275 and RDR6-SGS3 might be present simultaneously on the *PHAS* lncRNA. The
601 AGO1-miR2275 cleaved 5' unpaired portion may not go through immediate degradation. Red bar
602 represents the relative location of the VARNISH probe for *PHAS* lncRNA. Red boxes represent probe
603 locations for 24-nt phasiRNA 1 and 24-nt phasiRNA 2. smFISH probes are represented with dash lines.
604 (**B**) Comparison of sRNA-PAINT and smFISH for the same RNA transcript (*PHAS* lncRNA). sRNA-PAINT
605 detected a similar RNA localization pattern compared with smFISH, with increased single-molecule
606 resolution and a higher quantification count. All images were taken on the same coverslip sequentially.
607 Scale bar = 10 µm in all images. (**C**) Quantification analysis of image in panel A. sRNA-PAINT detected
608 more *PHAS* lncRNA than smFISH. Numbers show the binding events for each cell (90-pixel size diameter
609 circle in Picasso software) in different cell layers. 3 different locations in each specified cell layer were
610 taken for statistical analysis. Different letters indicate significant differences (Tukey's test; P < 0.05,
611 n=90).
612
613 *Figure 5. sRNA-Exchange-PAINT for detection of phasiRNA biogenesis components in premeiotic maize*
614 *anther.*
615 (**A**) Schematic of maize anther stage and comparison of material used in sRNA-seq and sRNA-PAINT
616 method. (**B**) Image of sRNA-Exchange-PAINT carried on five targets. Zoomed-in image of the boxed area
617 is shown on the right corner. miR2275 probes were linked with the P0 docking strand and represented
618 with green color. 24-nt phasiRNA 1 probe was linked with P1 docking strand and represented with blue
619 color. 24-nt phasiRNA 2 probe was linked with P2 docking strand and represented with cyan color.
620 miR166 probe was linked with P4 docking strand and represented with yellow color. *PHAS* lncRNA was
621 linked with P5 docking strand and represented with red color. (**C**) Comparison of the quantification
622 result of four target miRNAs using sRNA-seq and sRNA-qPAINT. Representative sRNA copy number
623 estimates were calculated by the sum of the binding sites shown in the boxed area using sRNA-qPAINT.
624 (**D**) Sequential detection of five targets and overlay with the nucleus. Overlay of the channels shows the
625 complexity and density of the small RNAs. Zoomed in image of the boxed area shows single-molecule

626 detection capability with higher-level of multiplexing. The imager strand in each channel is indicated
627 with the diagram above each image, and the quantification of binding sites of each channel is shown in
628 the white box.
629
630 **Supplementary Figure Legends**
631 *Supplementary Figure 1. sRNA-PAINT showed limited to no background with a scrambled control probe.*
632 (**A**) sRNA-PAINT with probes for a 24-nt phasiRNA and a scrambled control. Both docking strands were
633 detected with corresponding imager strands. Arrows indicate 2 out of ~66 fiducials used in experiments.
634 Scrambled control detected little or no signal. Scale bar = 10 µm for all images. (**B**) qPAINT analysis of
635 background level of LNA probes with scrambled controls. Number of the binding events for each
636 calculated area (20 pixel size diameter circle in Picasso software) in different cell layers were plotted. A
637 mean of 5.12 binding sites were calculated and used as background level for all subsequent calculations.
638 Ten locations in each cell layer were picked for qPAINT quantification. Three replicates and a total of 150
639 samples were used for the background calculation (n=150).
640
641 *Supplementary Figure 2. Quantification of specificity of VARNISH probes.*
642 VARNISH 24-nt phasiRNA probe (V), a probe with 2-nt mutations (m2), and probe no LNAs (nL) were
643 applied to each anther sample. Quantification was done using qPAINT analysis. Numbers show the
644 binding events for each cell in different cell layers. An average of 95% reduction is detected with m2 in
645 all cell layers. 10 different locations in each specified cell layer and three replicates (two replicates for
646 nL) were taken for statistical analysis (n=150 for V and m2, n=100 for nL). A no LNA probe with 2 nt
647 mutation was used as control for nL probe for qPAINT calculation. Letters indicate significant differences
648 using Tukey's test ($P < 0.05$).
649
650 *Supplementary Figure 3. VARNISH probe signals remain stable during imaging.*
651 Number of localization spots detected remain relatively stable during the imaging process of 20,000
652 frames for 24-nt phasiRNA.
653
654 *Supplementary Figure 4. sRNA-Exchange-PAINT for miR2275 and 24-nt phasiRNA co-localization.*
655 (**A**) A diagram showing sRNA-Exchange-PAINT, which differs from sRNA-PAINT via the use of multiple
656 imager strands. Imager strand 1 is first introduced to the sample, and after imaging, imager strand 1 is
657 removed with a buffer wash. Next, imager strand 2 is introduced. This process can be repeated until the

658 needed number of targets is reached. (**B**) sRNA-Exchange-PAINT on miR2275 (yellow) and a 24-nt
659 phasiRNA (blue) in maize anther. After the buffer wash, imaging showed little or no signal following each
660 round of detection using the imager strands. Scale bar = 10 µm for all images. (**C**) Merged and zoomed
661 image of the marked region is shown. These two sRNAs do not show significant co-localization at
662 nanometer resolution.
663
664 **Supplementary Tables**
665 *Supplementary Table 1. Information for sequential image of phasiRNA generation components using*
666 *sRNA-Exchange-PAINT*.
667
668 *Supplementary Table 2. Probes for smFISH of a* PHAS *precursor.*
669

Fig. 1

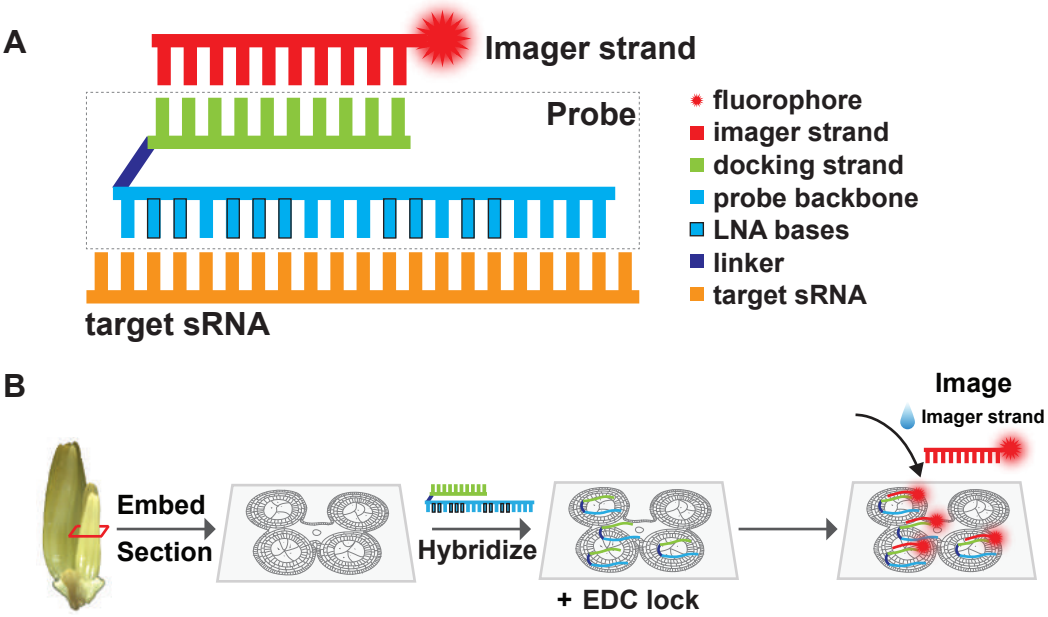
A
Imager strand
Probe
fluorophore
imager strand
docking strand
probe backbone
LNA bases
linker
target sRNA
target sRNA
B
Image
Imager strand
Embed
Section
Hybridize
+ EDC lock

Fig. 2

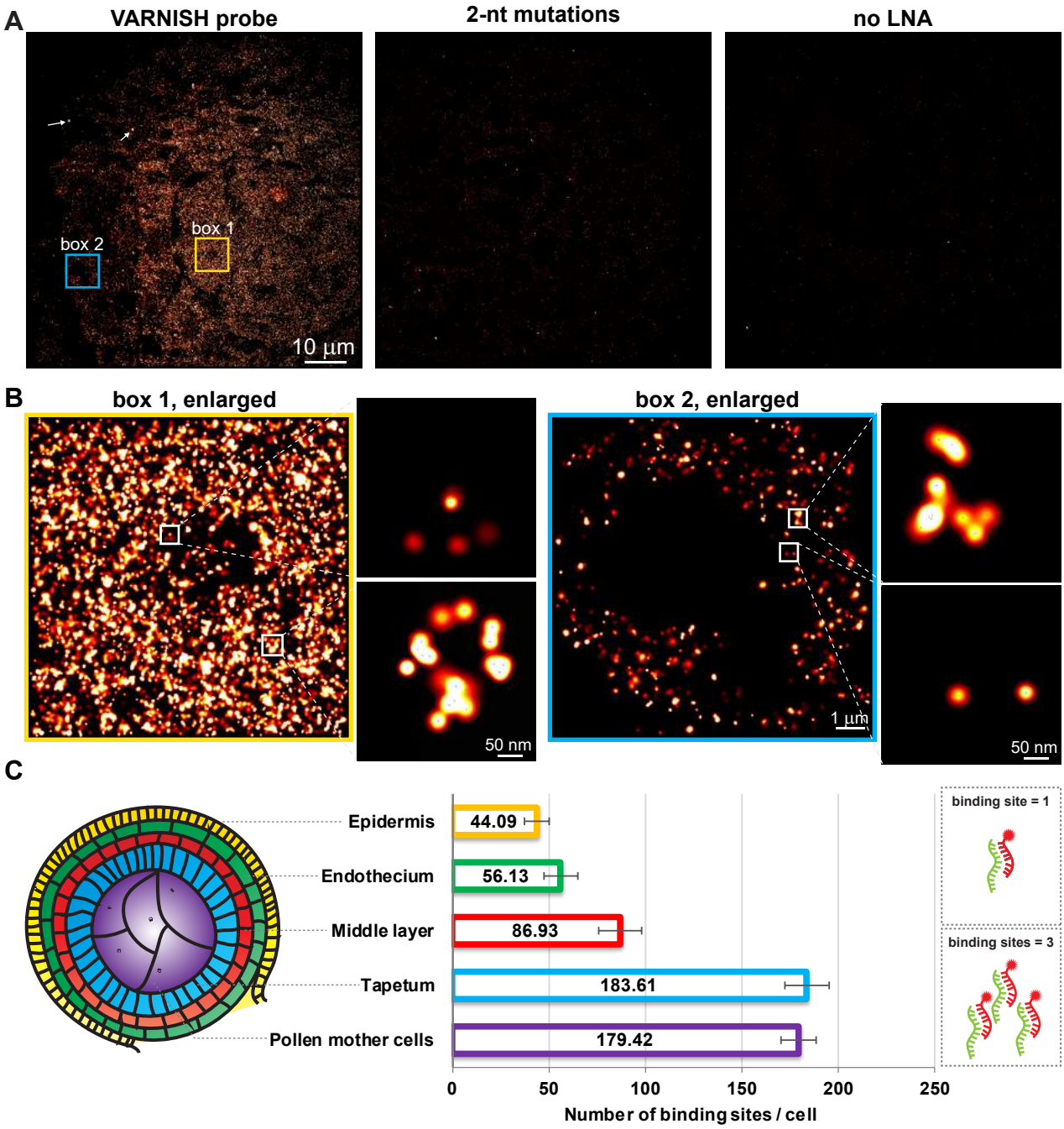
A
VARNISH probe
2-nt mutations
no LNA
box 1
box 2
10 µm
B
box 1, enlarged
box 2, enlarged
50 nm
1 µm
50 nm
C
Epidermis
Endothecium
Middle layer
Tapetum
Pollen mother cells
44.09
56.13
86.93
183.61
179.42
0
50
100
150
200
250
Number of binding sites / cell
binding site = 1
binding sites = 3

Fig. 3

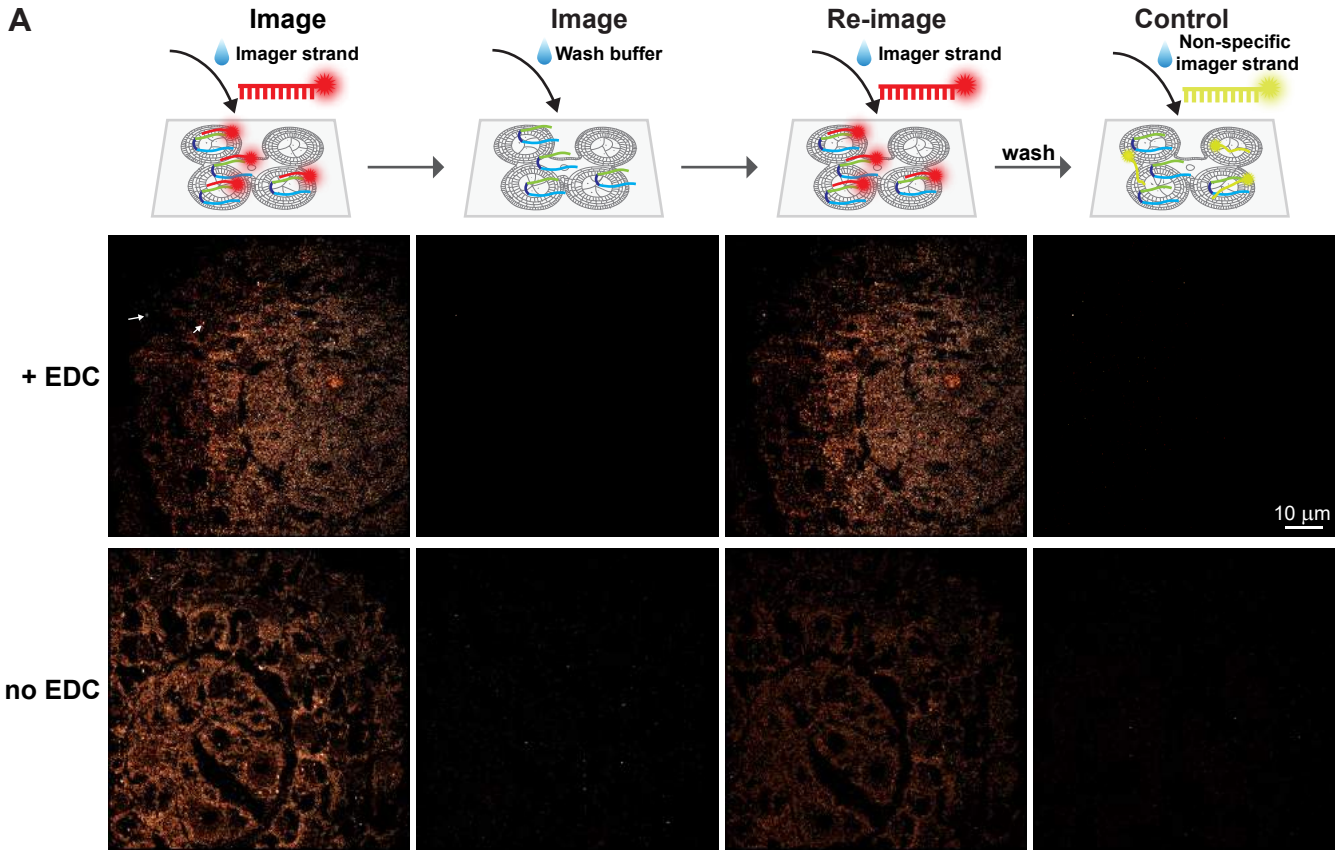
A
Image
Imager strand
Image
Wash buffer
Re-image
Imager strand
wash
Control
Non-specific imager strand
+ EDC
no EDC
10 µm

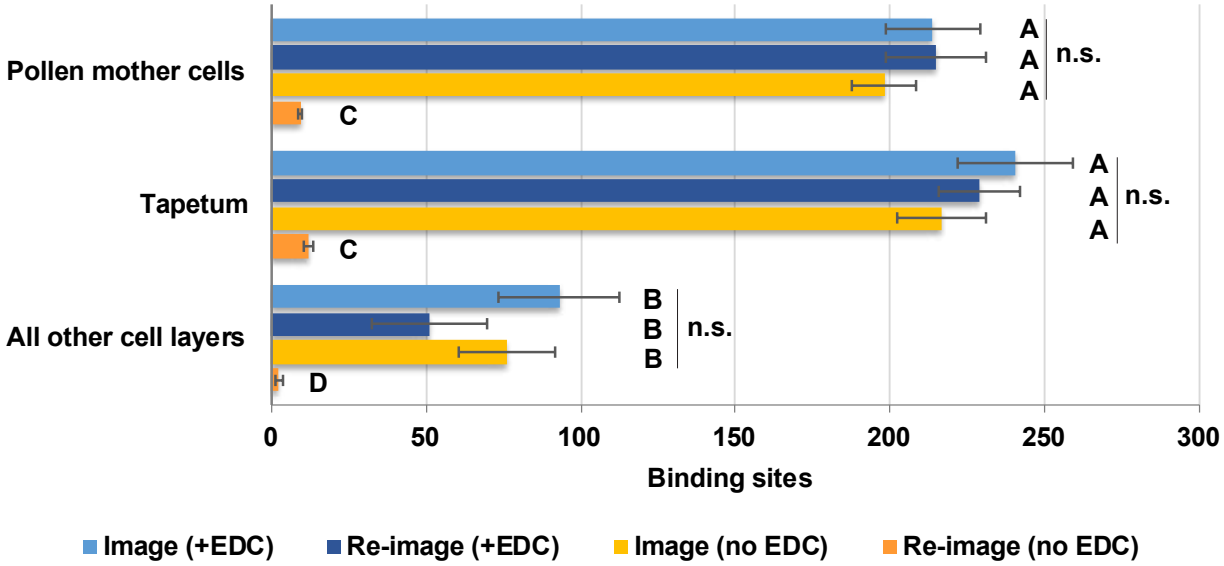
B
Pollen mother cells
Tapetum
All other cell layers
A
A
A
n.s.
C
A
A
A
n.s.
C
B
B
B
n.s.
D
0
50
100
150
200
250
300
Binding sites
Image (+EDC)
Re-image (+EDC)
Image (no EDC)
Re-image (no EDC)

Fig. 4

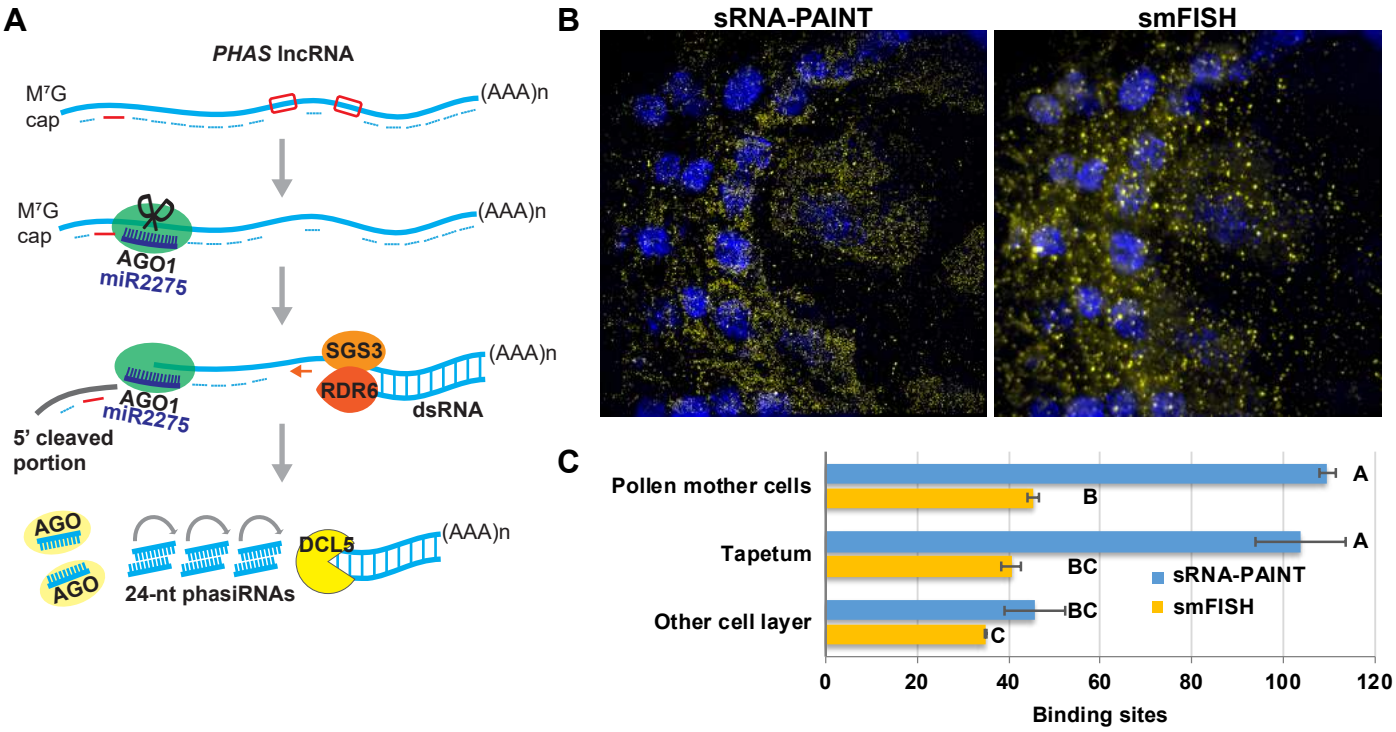
A
PHAS lncRNA
M7G cap
(AAA)n
AGO1
miR2275
SGS3
RDR6
dsRNA
5' cleaved portion
AGO
24-nt phasiRNAs
DCL5
B
sRNA-PAINT
smFISH
C
Pollen mother cells
Tapetum
Other cell layer
A
B
A
BC
BC
C
sRNA-PAINT
smFISH
0
20
40
60
80
100
120
Binding sites

Fig. 5

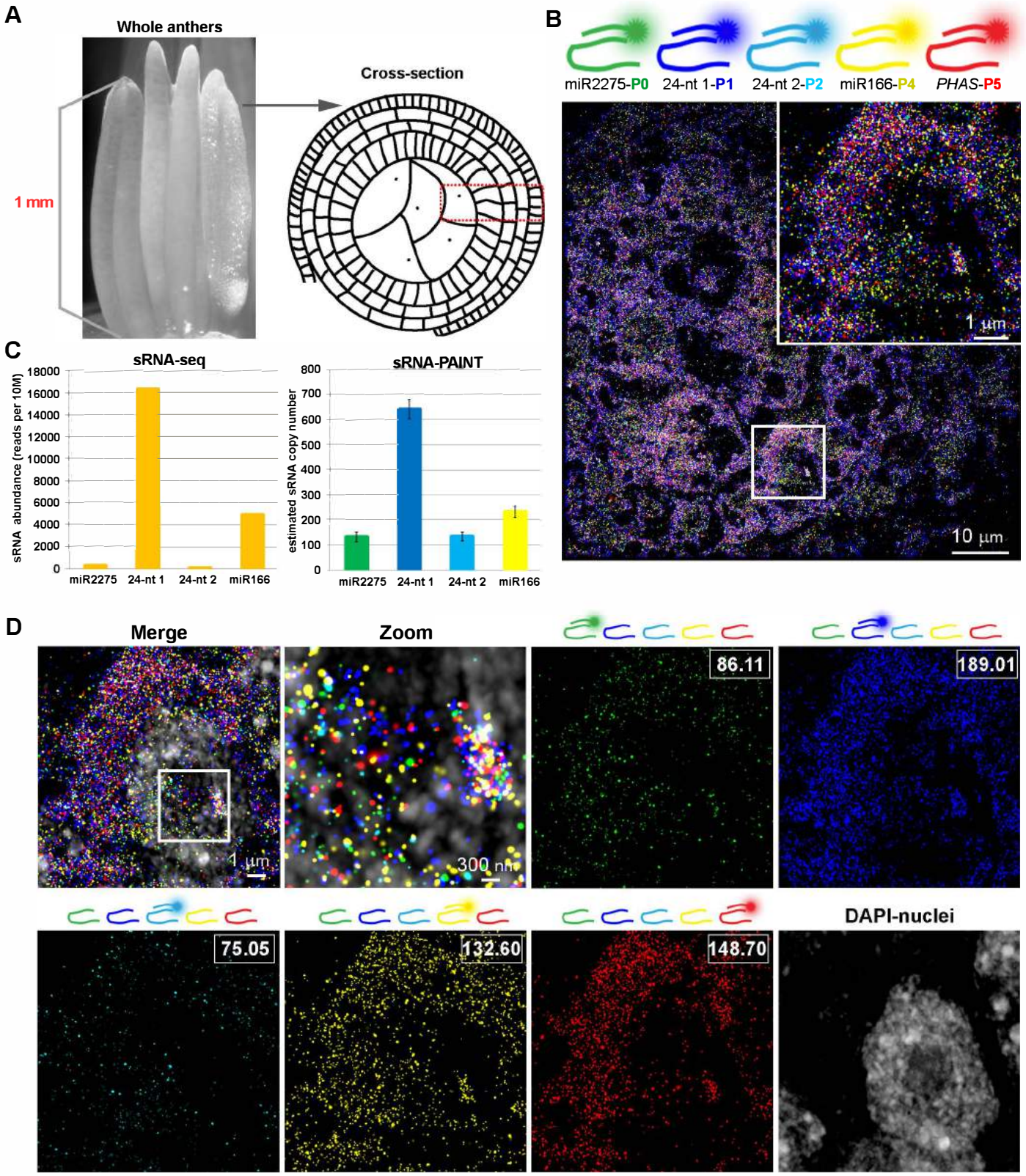
A
Whole anthers
1 mm
Cross-section
B
miR2275-P0
24-nt 1-P1
24-nt 2-P2
miR166-P4
PHAS-P5
1 µm
10 µm
C
sRNA-seq
sRNA abundance (reads per 10M)
18000
16000
14000
12000
10000
8000
6000
4000
2000
0
miR2275
24-nt 1
24-nt 2
miR166
sRNA-PAINT
estimated sRNA copy number
800
700
600
500
400
300
200
100
0
miR2275
24-nt 1
24-nt 2
miR166
D
Merge
Zoom
1 µm
300 nm
86.11
189.01
75.05
132.60
148.70
DAPI-nuclei

Supplementary Fig. 1

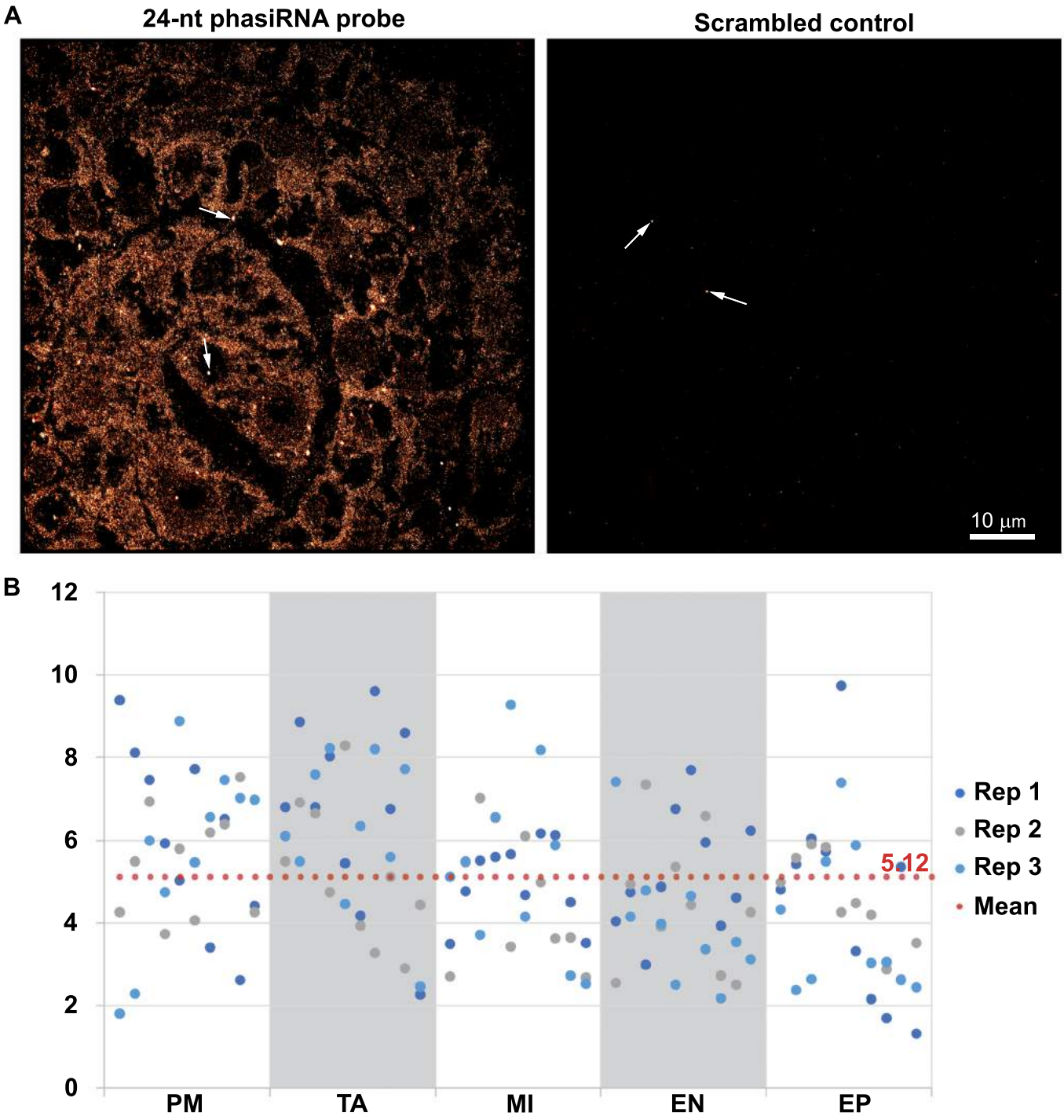

Supplementary Fig. 2

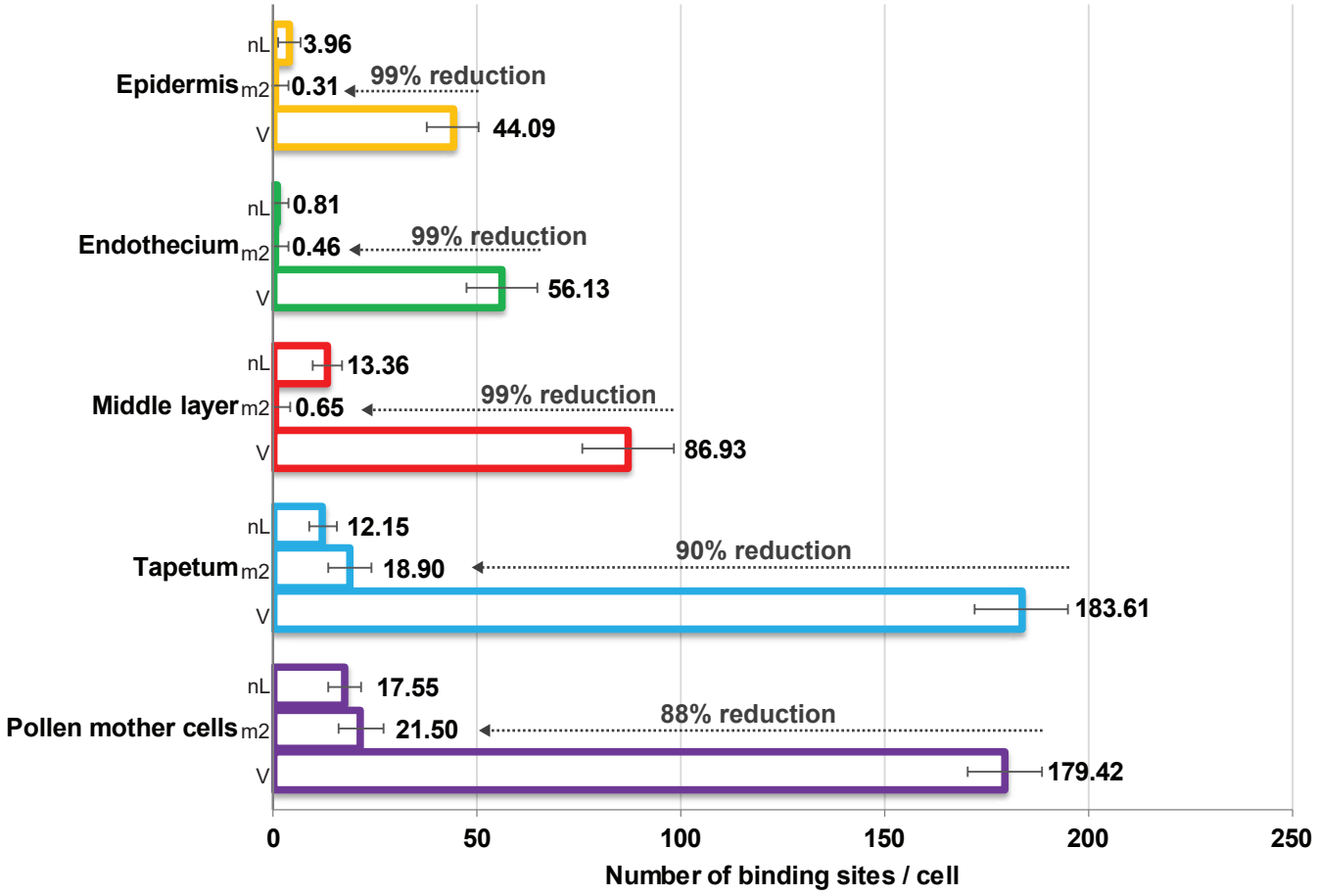

Supplementary Fig. 3

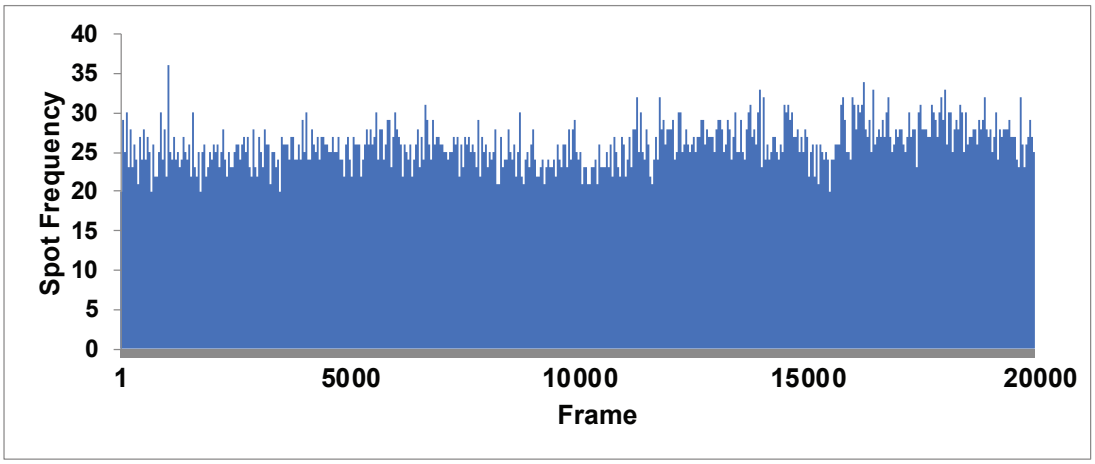
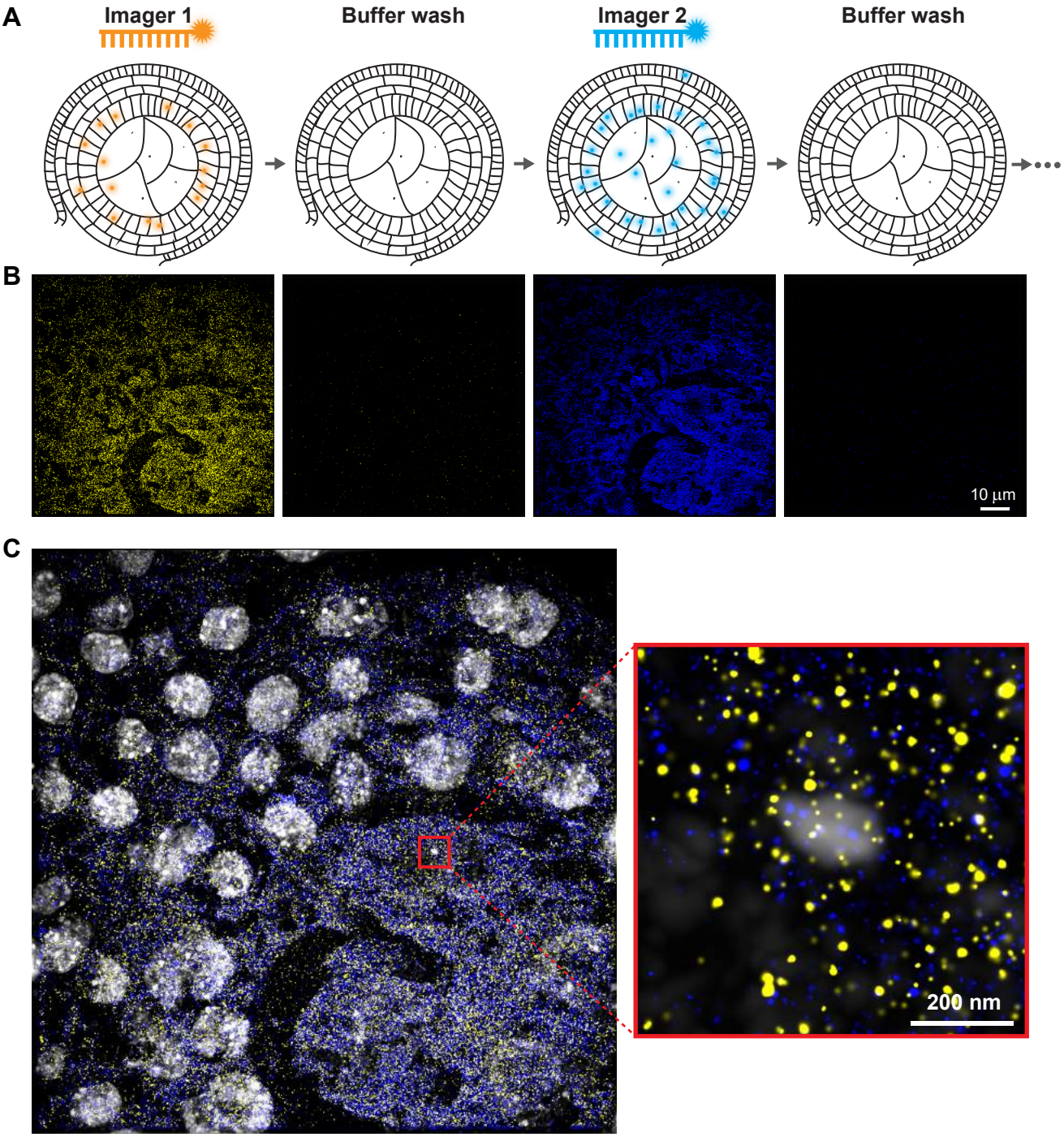
Supplementary Fig. 4